Direct Profiling and Reversibility of Ion Distribution at a Charged Membrane/Aqueous Interface: An X-ray Standing Wave Study

Jin Wang,*[,†,||] Martin Caffrey,*[,†] Michael J. Bedzyk,[‡] and Thomas L. Penner[§]

Biochemistry, Biophysics and Chemistry, The Ohio State University, Columbus, Ohio 43210, Materials Science Division, Argonne National Laboratory, Argonne, Illinois 60439, Department of Materials Science and Engineering, Northwestern University, Evanston, Illinois 60208, and Eastman Kodak Company, Rochester, New York 14650

Received November 6, 2000. In Final Form: March 22, 2001

Thermodynamic reversibility of ion binding at a membrane/aqueous interface has been demonstrated using variable period X-ray standing waves generated above a gold mirror. The interface consists of a negatively charged and polymerized phospholipid monolayer bathed in a dilute zinc chloride solution. Zinc ion distribution in the diffuse double layer was monitored as the pH of the aqueous medium was titrated from a value of 5.8 to 2.0 and back again to pH 5.8. The ion distribution was modeled by an exponentially decaying function. As H^+ concentration increased upon changing pH from 5.8 to 2.0, the amount of zinc in the diffuse double layer (integrated as a two-dimensional projection along the surface normal) decreased from 1.4×10^{13} to 1.0×10^{12} ions/cm^2 and the concentration of bound zinc at the surface dropped by a factor of 6.4 from an initial value of 122 mM to a low of ca. 19 mM. Recovery of the pH 5.8 distribution profile was essentially complete upon back-titration from pH 2.0. These results demonstrate clearly that within the experimental error of the measurement ion distribution at the charged membrane interface is reversible upon adjusting the pH of the electrolyte solution which corresponds to altering the degree of protonation and, thus, the net charge on the exposed phosphate headgroups.

Introduction

At a charged or polar surface immersed in an electrolyte solution, long-range electrostatic interactions dictate the formation of a concentrated ion layer, which can be understood as a charge screening effect. It is believed that the charge on the surface is offset by an equal and opposite charge afforded by counterions, some of which are transiently bound to the surface in the form of a Stern or Helmholtz layer, whereas others form a relatively thick overlayer of ions in rapid thermal motion close to the surface. The latter is referred to as the diffuse double layer.[1] To understand how a charged membrane interacts with an electrolyte solution and how the interfacial structure changes as a function of thermodynamic conditions constitutes a major challenge in many fields including electrochemistry, biophysics, and biochemistry. In the context of membrane electrostatics, it is expected that the charge, electrostatic potential, and ion distributions existing at a membrane/aqueous interface will modulate biological processes such as transport, electron transfer, enzyme activation, and membrane-protein topology.[2] Since the original work of Helmholtz, Gouy, Chapman, and Stern in which a framework for the diffuse double layer problem was established almost a century ago,[3−6] studies of interfaces of this type have tended toward a theoretical analysis of idealized and simple systems. It is only in the relatively recent past that experimental methods involving surface force, electric current or capacity, transport, and spectroscopic approaches have been used with a view to testing these theories and hypotheses. However, common to most existing methods is the shortcoming that they are indirect and of poor spatial resolution and, usually, require a host of simplifying assumptions in data analysis. The major difficulty associated with in situ measurement of this kind is the lack of an experimental probe of high resolution that can penetrate a layer of electrolyte solution above the charged membrane surface.

Because of their penetrating nature, X-rays have been used effectively in studying the structure of gas/liquid or liquid/solid interfaces. In the past, several X-ray techniques such as surface extended X-ray absorption fine structure (SEXAFS)[7,8] and in situ surface X-ray scattering[9−11] have been used to study electrochemical interfaces. SEXAFS can reveal the local chemical environment of a surface atom with subangstrom resolution, while surface X-ray scattering is most suited for studying in-plane, short- and long-range order in adsorbed surface atomic and molecular layers. However, both methods can be applied effectively only to samples with strong X-ray absorption or scattering centers as prevail in densely packed, heavy atoms/ions at an electrode surface. Also, these techniques do not provide information on ion distribution on a nanometer length scale and beyond in the direction normal to the interface. Recently, the

† The Ohio State University.
‡ Argonne National Laboratory and Northwestern University.
§ Eastman Kodak Company.
|| Present address: Advanced Photon Source, Argonne National Laboratory, Argonne, IL 60439.

(1) Israelachvili, J. N. *Intermolecular & Surface Forces*, 2nd ed.; Academic Press: San Diego, 1991.
(2) Blank, M. In *Electrical Double Layers in Biology*; Blank, M., Ed.; Plenum: New York, 1986.
(3) von Helmholtz, H. L. F. *Ann. Phys.* **1853**, *89*, 211.
(4) Gouy, G. *J. Phys. Radium* **1910**, *9*, 457.
(5) Chapman, D. L. *Philos. Mag.* **1913**, *25*, 475.
(6) Stern, O. H. *Z. Elektrochem.* **1924**, *30*, 508.
(7) Blum, L.; Abruna, H. D.; White, J.; Gordon, J. G.; Borges, G. L.; Samant, M. G.; Melroy, O. R. *J. Chem. Phys.* **1986**, *85*, 6732.
(8) Abruña, H. D. In *Electrochemical Interfaces*; Abruña, H. D., Ed.; VCH: New York, 1991.
(9) Dahn, J.; Py, M. A.; Haering, R. R. *Can. J. Phys.* **1982**, *60*, 307.
(10) Chianelli, R. R.; Scanlon, J. C.; Rao, B. M. L. *J. Electrochem. Soc.* **1978**, *125*, 1563.
(11) Toney, M. F.; Melroy, O. R. In *Electrochemical Interfaces*; Abruña, H. D., Ed.; VCH: New York, 1991.

10.1021/la001542x CCC: $20.00
Published on Web 06/05/2001

counterion overlayer formed at the interface between an electrolyte solution and a monolayer of a carboxylic acid terminated alkane thiol self-assembled on gold crystals has been studied by X-ray reflectivity.[12] In this study, the amount of bound cadmium counterion at the charged surface was shown to be sensitive to the pH of the electrolyte solution. The density of cadmium in the overlayer increased monotonically as the electrolyte was titrated from pH 3.9 to 8.5. However, cadmium binding was not reversible upon back-titration. X-ray evanescent waves have been used to study the concentration profile of polymeric materials near a gas/liquid interface on a length scale of tens to thousands of angstroms,[13] but the intrinsic spatial resolution of the method limits its utility in studies requiring detailed structural characterization. Finally, measurement of the diffuse double layer constrained between charged phospholipid membranes has been made by neutron[14] and X-ray[15] diffraction.

In the recent past, the X-ray standing wave (XSW) method has been used to probe structural features of electrode/aqueous and membrane/aqueous interfaces. In the former study, the electrodeposition of copper on an iodine-treated platinum surface along with the redox properties of a self-assembled monolayer (SAM) at a platinum (Pt/PtO) electrode was examined.[16] In the latter study, zinc ion distribution in an electrolyte solution in contact with a charged, polymerized phospholipid membrane was profiled directly.[17] The experimental results agreed qualitatively with the Gouy−Chapman−Stern theories of membrane electrostatics. It was found that the charged surface was partially neutralized by a condensed (or adsorbed) layer of counterions and that ion distribution in the adjacent solution formed a diffuse layer decaying with an exponential functional form. The zinc ion distribution was found to be sensitive to headgroup charge density manipulated experimentally by adjusting the pH of the electrolyte solution. However, thermodynamic reversibility of surface charge density and of ion distribution was not examined. This represents the focus of the current study where we use variable period XSWs generated above a gold mirror surface as a probe to profile the pH-dependent zinc distribution at the membrane/aqueous interface as described previously.[17] In this report, a more complete treatment of the background theory, experimental methods, and data analysis is presented than was possible in the earlier paper.

Background

Diffuse Double Layer. The one-dimensional Poisson−Boltzmann (PB) equation has long been used to describe the electrostatic potential near a charged surface in an electrolyte solution. The equation has the form

$$\frac{d^2\psi(z)}{dz^2} = -\frac{e}{\epsilon\epsilon_0}\sum_i c_i N_i(z) \qquad (1)$$

where ψ is the electric potential normal to the charged surface along the z-direction, e is the elementary charge, $\epsilon\epsilon_0$ is the dielectric constant of the electrolyte solution (the value of which is close to that of water in dilute solutions), and c_i is the valency and $N_i(z)$ is the concentration of type i ions at a distance z from the charged surface. The concentration of ion, i, at z satisfies the Boltzmann distribution:

$$N_i(z) = N_{bi}\exp\left[-\frac{ec_i\psi(z)}{kT}\right] \qquad (2)$$

where N_{bi} is the bulk concentration of ion species, k is the Boltzmann constant, and T is temperature. The solution to the PB equation gives the potential, electric field, and ion density at any distance from the charged surface. For low surface electric potentials (for example, $\psi_0 \ll 25/c_i$ mV at room temperature), the PB equation (eq 1) can be simplified by linear expansion to a linear equation of the form

$$\frac{d^2\psi(z)}{dz^2} = \kappa^2\psi(z) \qquad (3)$$

where

$$\kappa = \sqrt{\sum_i N_{bi}e^2{c_i}^2/\epsilon\epsilon_0 kT} = \sqrt{Se^2/\epsilon\epsilon_0 kT} \qquad (4)$$

and S ($=\sum_i N_{bi}c_i^2$) is the ionic strength of the bulk solution. κ^{-1} is the Debye or screening length, L, of the electrostatic potential and is a characteristic length or thickness of the diffuse double layer. In this approximation, the potential has an exponential decaying functional form:

$$\psi(z) = \psi_0\exp(-\kappa z) \qquad (5)$$

where ψ_0 is an integration constant representing the potential at the surface and is determined by the boundary conditions. The ion concentration distribution can be obtained by substituting eq 5 into eq 2:

$$N_i(z) = N_{bi}\exp\left[-\frac{ec_i\psi_0}{kT}\exp(-\kappa z)\right] \qquad (6)$$

This "hyperexponential" function for the ion distribution (eq 6) can have a much shorter decay length than that of the simple potential function shown in eq 5. In a further linear approximation under conditions of low surface potential, that is, where $ec_i\psi_0/kT\exp(-\kappa z) \ll 1$, ion distribution in the diffuse double layer close to the charged surface reduces to a simple exponential function:

$$N_i(z) = -\frac{ec_i N_{bi}\psi_0}{kT}\exp(-\kappa z) + N_{bi} = N_{si}\exp(-\kappa z) + N_{bi} \qquad (7)$$

where N_{si} is the ion concentration at the charged surface ($N_i(0)$) over and above the bulk concentration:

$$N_{si} = -\frac{ec_i N_{bi}\psi_0}{kT} = N_i(0) - N_{bi} \qquad (8)$$

It should be emphasized that eq 7 can be derived only with the assumption that the surface potential is low ($\psi_0 \ll 25/c_i$ mV at room temperature). In general, the solution of the nonlinear PB equation (eqs 1 and 2) gives the potential and charge distribution of a diffuse double layer. However, the solution in an analytical form is available

(12) Li, J.; Liang, K. S.; Scoles, G.; Ulman, A. *Langmuir* **1995**, *11*, 4418.
(13) Bloch, J. M.; Sansone, M.; Rondelez, F.; Peiffer, D. G.; Pincus, P.; Kim, M. W.; Eisenberger, P. M. *Phys. Rev. Lett.* **1985**, *54*, 1039.
(14) Hentschel, M. P.; Bueldt, G.; Oberthur, R. C.; Mischel, M. *FEBS Lett.* **1985**, *193*, 236.
(15) Kirchner, S. *Biochim. Biophys. Acta* **1996**, *1279*, 181.
(16) Abruña, H. D.; Bommarito, G. M.; Acevedo, D. *Science* **1990**, *250*, 69.
(17) Bedzyk, M. J.; Bommarito, G. M.; Caffrey, M.; Penner, T. L. *Science* **1990**, *248*, 52.

only for electrolyte systems of simple composition (for example, 1:1 and 1:2 electrolytes).[1,18]

Even with an exact solution for the nonlinear PB equation, the diffuse double layer is highly idealized. A membrane, exposed to an aqueous solution, such as prevails in our study, can hardly be described as a rigid, infinitely smooth, and uniformly charged surface. The phospholipid monolayer that is actually being studied has flexible headgroups that are individually charged and is microscopically rough. Further, the membrane/aqueous solution interface is probably permeable to a certain extent. These effects can modify the potential and ion distribution in the membrane/electrolyte interfacial region.[19−22]

For simplicity, we chose an exponential function (eq 7) to model the ion distribution in the diffuse double layer. Model selection and its impact on the fitting results are discussed more completely under Discussion.

X-ray Standing Wave Method. XSWs are generated when the plane waves of an X-ray beam striking a reflecting or diffracting optical element interfere with the corresponding reflected or diffracted plane waves. In the current application, X-ray standing waves generated by total external reflection were used. The principle of the XSW method has been described in detail previously.[23,24] In what follows, a brief introduction to the terms used in discussing XSW in this article will be presented.

For X-rays in most materials, the index of refraction n is less than unity:

$$n = 1 - \delta - i\beta \tag{9}$$

where δ and β refer to the refractive index decrement and the absorption index of the X-rays in the medium, respectively, and are small quantities of magnitude $<10^{-5}$. Analogous to the total internal reflection associated with visible light, an X-ray beam striking a vacuum/mirror interface will undergo total external reflection when the incident angle θ is below the critical angle θ_c. θ_c is defined as $\sqrt{2\delta}$ which is in the range of several milliradians (mrad, 1 mrad = 0.057°) for most materials and X-ray energies. The period D of the standing wave generated by the interference of the coherently related incident and reflected plane waves is $\lambda/(2 \sin \theta)$, where λ is the X-ray wavelength. The period of the XSW at θ_c is referred to as the critical period D_c ($= \lambda/(2 \sin \theta_c)$). For all practical purposes, D_c is energy-independent and depends on the electron density of the mirror material. D_c of a gold mirror in vacuo is 80 Å. At an incident X-ray photon energy of 9.9 keV, θ_c is 7.67 mrad.

The angular (θ) and positional (z) dependence of the XSW electric field (E-field) intensity in a vacuum above a mirror surface can be expressed as[23]

$$I(\theta,z) = I_0\left[1 + R(\theta) + 2\sqrt{R(\theta)}\cos\left(\nu - 2\pi\frac{z}{D}\right)\right] \tag{10}$$

where I_0 is the E-field intensity of the incident X-ray beam, R is the reflectivity of the X-ray mirror surface, and ν is the relative phase of the reflected plane wave at the surface. ν decreases from π to 0 as θ is increased from 0 to θ_c. Thus, by an increase in θ, the standing wave moves in the direction of the surface and the exact E-field profile above the surface can be calculated over the entire θ range. The distribution, $\rho(z)$, of a layer of marker or probe atoms suspended above the mirror surface in or on an organic thin film or liquid can be determined by recording the X-ray fluorescence, Y, from the marker atom layer as a function of θ:

$$Y(\theta) = \int I(\theta,z)\,\rho(z)\,\mathrm{d}z \tag{11}$$

where $Y(\theta)$ is referred to as the fluorescence yield profile. This is made possible by virtue of the fact that the photoelectric effect, evidenced by X-ray fluorescence, is minimized and maximized when the nodes and antinodes, respectively, of the XSW are brought into coincidence with the marker atom layer during a scan in θ. Given that $I(\theta,z)$ can be calculated exactly, the position of a marker atom layer above the mirror surface can be located by numerically fitting the measured X-ray fluorescence yield profile with calculated profiles assuming a model-dependent marker atom distribution $\rho(z)$ (see Experimental Aspects: XSW Data Analysis). Further, for a well-defined marker atom layer, its position can be estimated roughly by counting the number of peaks in a fluorescence yield profile below θ_c. Thus, a profile with X modulations below θ_c has a heavy atom layer situated at $(X - 0.5)D_c$ above the mirror surface.

Experimental Aspects

Sample Preparation. The structure and composition of the sample used in this study are shown in Figure 1. A gold mirror (Liberty Mirrors, Brackenridge, PA), which has a critical angle of 7.67 mrad at 9.9 keV, was employed to generate the XSWs and as a solid substrate for the organic monolayers. The gold and chromium films in the mirror were thermally evaporated onto float glass slides with gold as the top layer. The lipid monolayers were prepared at the Corporate Research Laboratories of the Eastman Kodak Co. as follows. The gold mirror (1.25×2.50 cm^2) was plasma-cleaned (model PDC-3XG, Harrick Scientific Corp., Ossining, NY; argon pressure, <1.0 Torr; high power setting) for less than 2 min to expose a fresh gold surface. After cleaning, the substrate was immediately immersed in 1 mM octadecanethiol (ODT) in freshly distilled tetrahydrofuran (THF) and incubated at room temperature for ca. 12 h. The thickness of the chemically adsorbed ODT monolayer was 21 ± 0.5 Å measured by ellipsometry (model L116C, Gaertner Scientific Corp., Chicago, IL). Further, the advancing contact angle of a water droplet on the surface was monitored using a goniometer scope (model 100-04, Rame-Hart Inc., Mountain Lakes, NJ) by way of characterizing the hydrophobic surface. The contact angle was 102° after ODT treatment indicating an extremely hydrophobic surface.

The polymerizable phospholipid, bis[8-(octadeca-2,4-dienoyl)-octyl]-phosphate (see Figure 1) was deposited using the LB technique.[25] In a KSV 2200 LB system, the phospholipid was spread and compressed to a condensed monolayer at a surface pressure of ca. 30 mN/m on a 3×10^{-4} M zinc chloride aqueous solution subphase. The compressed phospholipid monolayer at the air/water interface was allowed to equilibrate for 30 min. The LB monolayer of the phospholipid was deposited onto the hydrophobic gold mirror during its first vertical downstroke at a rate of 3 mm/min. The transfer ratio was close to unity indicating quantitative monolayer deposition. The remaining film floating on the water surface was removed by aspiration. The lipid-coated gold mirror was rotated until it was facing and parallel to but still below the subphase surface. The LB monolayer was then polymerized by irradiation with 254 nm light for 5 min while

(18) Cevc, G.; Marsh, D. *Phospholipid Bilayers*; Wiley: New York, 1987.
(19) Cevc, G.; Svetina, S.; Zeks, B. *J. Phys. Chem.* **1981**, *85*, 1762.
(20) Kirchner, S.; Cevc, G. *J. Chem. Soc., Faraday Trans.* **1994**, *90*, 1941.
(21) Lennard-Jones, J. E.; Dent, B. M. *Trans. Faraday Soc.* **1928**, *24*, 92.
(22) Belaya, M.; Levadny, V.; Pink, D. A. *Langmuir* **1994**, *10*, 2010.
(23) Bedzyk, M. J.; Bommarito, G. M.; Schildkraut, J. *Phys. Rev. Lett.* **1989**, 1376.
(24) Wang, J.; Caffrey, M.; Bedzyk, M. J.; Penner, T. L. *J. Phys. Chem.* **1994**, *98*, 10957.
(25) Roberts, G. G. *Contemp. Phys.* **1984**, *25*, 109.

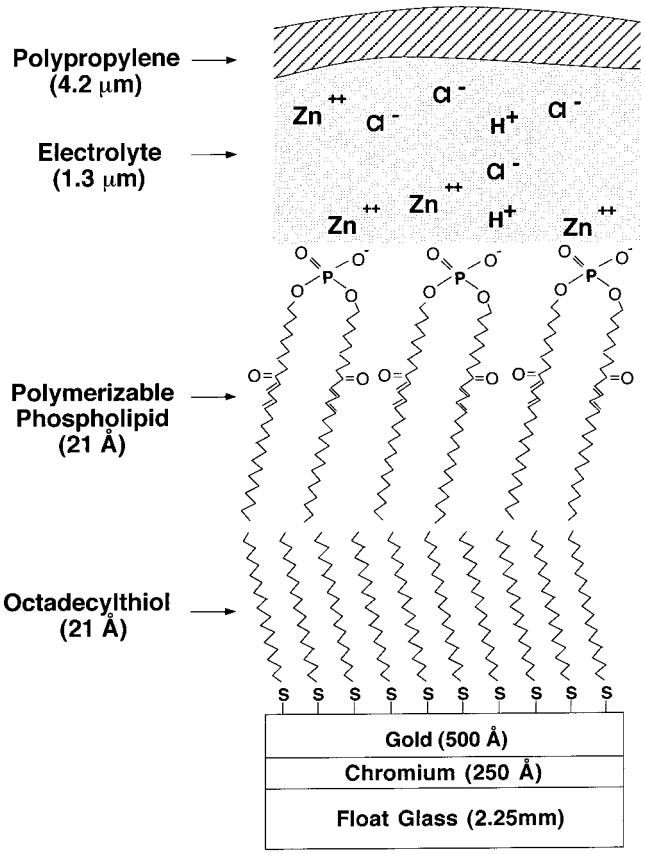

Figure 1. Schematic of the gold mirror, deposited films, electrolyte solution, and plastic cover used in determining zinc ion distribution in the diffuse double layer by means of the XSW method. The gold mirror surface was rendered hydrophobic with an ODT self-assembled monolayer before deposition of a bis[8-(octadeca-2,4-dienoyl)octyl]-phosphate monolayer using the LB technique. Details of the phospholipid deposition and photopolymerization procedures are described in the text. The phospholipid structure shown here is that of the monomer before polymerization. The exact structure of the polymerized product is not known. The dimensions included in the schematic were obtained from ellipsometry in the case of the deposited SAM and LB organic monolayers and from the manufacturer's specifications in the case of the gold mirror and the prolene film. The thickness of the encapsulated 0.1 mM zinc chloride solution is typical of values determined from the reflectivity measurement (see text for details). The schematic is not drawn to scale.

remaining ca. 3 mm below the subphase surface during the exposure. After polymerization, the sample was returned to a vertical position and was withdrawn through the subphase surface at a speed of 10 mm/min. Ellipsometry showed that the polymerized phospholipid monolayer had a thickness of 21 Å. Before the XSW measurements, the sample was rinsed with a hydrochloric acid solution (pH 2.0) to remove zinc ions associated with the phospholipid headgroup. By polymerization of the LB film, the sample could be removed intact from the water subphase even though it has a charged, hydrophilic headgroup exposed to air. Failure to polymerize resulted in a loss of half of the monolayer upon withdrawing the substrate through a clean subphase surface. Polymerization is probably also important in allowing the sample to survive the extensive acid and water rinsing and subsequent reimmersion for the XSW measurements.

Sample Cell. Sample holder design is critical to the success of this study because of the in situ nature of the measurements and the severe geometric requirements for generating XSWs. The cell used in this experiment was based on the design of Samant et al.[26] With reference to Figure 2, the body of the cell was made of Teflon and incorporated inlet and outlet ports through which the various bathing and washing solutions flow. The substrate bearing the polymerized phospholipid monolayer was placed on top of the Teflon cell, and the entire unit was covered with a 4.2 μm thick prolene film (Chemplex Industries, Inc., Tuckahoe, NY), held tight and in place by an outer Teflon ring. Before the XSW measurement was made, the appropriate aqueous solution was flushed over the sample surface below the prolene film and was left to equilibrate for >15 min. To reduce the thickness of the aqueous solution above the sample to a minimum, a negative pressure was applied and maintained in the sample compartment by means of a compact vacuum pump during the XSW experiments. Under such circumstances, the measured water thickness was typically between 1 and 2 μm.

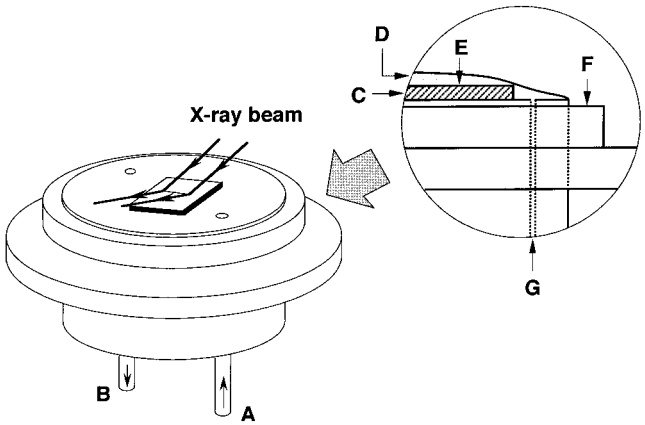

Figure 2. Schematic of the sample cell used for in situ XSW measurements of zinc ion distribution in the diffuse double layer. A and B identify the inlet and outlet for the electrolyte solution, respectively; C is the X-ray mirror and the SAM and LB films as shown in Figure 1; D is the 4.2 μm thick prolene film; E is the electrolyte solution; F is a Teflon ring that fits over the Teflon center piece to fix the prolene film firmly in position; G is one of two channels continuous with either A or B for supplying or removing the electrolyte solutions. This arrangement positions the sample surface slightly above the edge of the cell. Before an XSW scan was made, an appropriate volume of solution was flushed over the sample surface to ensure complete replacement of the old solution with the new. During the course of an XSW scan, a negative pressure was applied to A and B by means of a compact vacuum pump to remove excess solution above the sample surface.

XSW Measurements. The XSW measurements were performed on the D-line at the Cornell High Energy Synchrotron Source (CHESS) with the Cornell Electron-Positron Storage Ring (CESR) operating at 5.3 GeV and 35−47 mA total positron current. The experimental setup for the XSW measurements has been described previously.[17,24] The bending magnet synchrotron radiation was tuned to 9.9 keV by a pair of flat germanium (111) crystals in order to optimally excite the zinc K-fluorescence and to distance the scattering peak sufficiently far away in energy from the zinc Kα peak. The monochromator had an energy resolution of ca. 5 eV at 9.9 keV and a vertical divergence of less than 0.1 mrad (5.7 millidegrees). The monochromated beam was collimated to 30 μm in height and 4.5 mm in width by an $X-Y$ slit pair. The typical incident X-ray intensity at the sample surface under the above experimental conditions was 10^7 photons/s. Under these conditions, X-ray fluorescence from and reflectivity of the sample were recorded simultaneously at each incident angle. The data collection method and procedure have been described in detail previously.[24,27−29]

A series of XSW and reflectivity measurements were carried out with the sample at the following pH values and in the following order: 5.8, 4.2, 2.0, 4.2, and 5.8. The bathing medium consisted

(26) Samant, M.; Melroy, O. R.; Toney, M. F.; Borges, G. L.; Blum, L. *Surf. Sci.* **1988**, *193*, L29.

(27) Bedzyk, M. J. *Synchrotron Radiat. News* **1990**, *3*, 25.

(28) Wang, J. Ph.D. Thesis, The Ohio State University, Columbus, OH, 1994.

(29) Kirchner, S.; Wang, J.; Yin, Z.; Caffrey, M. *J. Appl. Phys.* **1995**, *78*, 2311.

of a 0.1 mM zinc chloride solution whose pH was adjusted by using hydrochloric acid.

In the course of conducting these in situ XSW measurements, strong inelastic scattering was encountered from the prolene film and from the solution bathing the sample. This had the effect of lowering the signal/noise ratio (S/N) in comparison with previous dry, exposed samples. Thus, to achieve acceptable counting statistics, a long counting time (between 3 and 5 min at each incident angle) was necessary. Accordingly, a θ-scan consisting of 64 angular steps required about 3−5 h to complete. To work within the confines of short fill times at CHESS which were typically less than 2 h long, multiple short but complete θ-scans from 0 to 15 mrad were recorded and subsequently summed at each pH value.

XSW Data Analysis. As described above, reflectivity and fluorescence data were collected simultaneously during each θ-scan. The reflectivity profiles were used to obtain information on interfacial roughness of the stratified sample and on the thickness of the encapsulated electrolyte solution layer as follows.

(1) Interfacial Roughness. Initially, a layered model of refractive index was proposed based on what was known about the structure of the sample. When the interfacial roughness was taken into account, two models were used for the different interfaces in the thin film system. First, the Debye−Waller (DW) model[30] was applied to all well-defined solid/solid interfaces under the electrolyte solution layer. The second model, the so-called Névot−Croce (NC) approximation,[31] was used to treat interfaces which are macroscopically rough including those associated with the air, prolene, and electrolyte layers. With the latter model, interfaces are described as regions with continuously changing refractive index. The function describing how the reflective index varies in the direction normal to the interface (the z-direction) is

$$F(z) = \frac{1}{\sigma\sqrt{2\pi}} \int_{-\infty}^{z} \exp\left(-\frac{z'^2}{2\sigma}\right) dz'^2 \qquad (12)$$

where σ is the root-mean-square (rms) roughness at the interface. For purposes of these calculations, an interface region is divided into many thin slabs with refractive indices equal to the value given by eq 12 at the center of each slab. The number and thickness of the slabs are chosen so that the resonance effect,[32] normally occurring in thick (>1000 Å) overlayers atop an X-ray reflecting mirror, is greatly lessened. In our calculation, each slab is 200 Å thick and 100 slabs for the air/film interface and 25 slabs for the film/solution interface were used.

(2) Exact Thickness of the Encapsulated Electrolyte Solution Layer. When X-rays strike a bare mirror surface, the reflectivity is close to unity until the incident angle increases to θ_c. However, if the mirror is covered with X-ray-absorbing layers, the measured reflectivity can drop dramatically at angles well below θ_c. The optical path length d_o of an X-ray beam in an absorbing overlayer at incident angle θ can be evaluated roughly by

$$d_o = \frac{2t_o}{\sqrt{\theta^2 - 2\delta_o}} \qquad (13)$$

where t_o is the thickness and δ_o is the refractive index increment of the overlayers. When t_o is on the order of a few micrometers, d_o can be as large as several centimeters for $\theta \ll \theta_c$. In the present study, the reflectivity is typically only 50% in this angular region indicating a considerable attenuation in the overlayers. Fitting the theoretical reflectivity to the experimental reflectivity profile yields the electrolyte solution thickness with a sensitivity of about 200 Å. In the calculation, the optical constants of the prolene layer including the refractive index increment and the absorption index were calculated according to the thickness (4.2 μm) and specific gravity (0.9 g/cm^3) provided by the manufacturer.

A χ^2-fitting procedure[33] was used to fit the theoretical reflectivity derived from the Fresnel equations[34] to the experimental curve by adjusting the interfacial roughness value in the DW and NC models and the electrolyte solution thickness. The values yielding the best fit were used in the subsequent E-field intensity and fluorescence calculations.

The entire fluorescence spectrum was available for data analysis when the ADC/histogram memory modules were used in data collection. Because of the fact that the zinc Kα peak at 8.6 keV sits on the shoulder of the scattered X-rays centered at 9.9 keV, an accurate measure of total fluorescence counts was obtained by evaluating the area beneath the zinc Kα peak using a χ^2-fitting program. The curve fitting consisted of a Gaussian on a quadratic background. The integrated fluorescence intensity data extracted from the spectrum was then corrected for the detector/spectrum amplifier dead time by a live-time factor (normally larger than 75%) which is the ratio of the pulser counts recorded in the spectrum and the input pulser counts. This correction is needed because of the finite response time of the detector and the amplifier such that a part of the incident events (standard pulser and fluorescence photons) go unamplified and are not recorded.

At low incident angles, $\theta < (h/H)$, where h is the beam height and H is the length of the sample along the X-ray beam, the footprint of the X-ray beam on the sample is fixed and of magnitude H. Beyond this angle, the length of the footprint l decreases monotonically with θ. Specifically,

$$l = \frac{h}{\theta} \qquad (14)$$

As a result, a smaller fraction of the film is illuminated by the X-ray beam as θ increases. A correction for this geometric effect was applied to the experimental data so that the fluorescence yield at each incident angle reported originates from a fixed sample area.

The distribution of zinc atoms in the electrolyte solution at and next to the phospholipid monolayer was determined by matching a theoretical model to the experimental data. The model distribution of zinc consisted of an exponentially decaying distribution close to the surface and an extended flat background in the micrometer thick solution layer. Specifically, the ionic concentration in the vicinity of the membrane/aqueous interface was modeled as

$$N(z) = N_s e^{-(z-z_0)/L} + N_b \qquad (0 < z - z_0 < d_w) \qquad (15)$$

where N_s is the zinc concentration at the membrane surface located at z_o above the mirror surface, L is the decay length or the effective Debye length of the zinc diffuse layer, N_b is the zinc concentration in the bulk solution, and d_w is the solution thickness. Both z_0 and L were adjustable parameters in the fitting protocol. Another fitting parameter was the ratio of N_s and N_b. Because the absolute value of N_b is known (0.1 mM), N_s can be determined from the fitting results. The fits were executed automatically until the minimum χ^2 value was reached. The fluorescence data in the angular range of 2.5−7.5 mrad were used in the fitting procedures.

We note that neither the E-field intensity distribution nor the fluorescence yield profile is particularly sensitive to the model distribution of optical indices in and near the organic films.[28] Thus, after a reasonable model was chosen for the sample at a certain pH, an iterating correction of the model because of changes in zinc distribution was not considered necessary and was omitted from the program.

Results

The angular dependence of the reflectivity and zinc Kα fluorescence data along with the theoretical fit for the sample at different stages during the pH titration is shown in Figure 3. The pH values are indicated as appropriate and the symbols "−" and "+" are used to distinguish the same pH accessed during titration to low and high pH

(30) de Boer, D. K. G. *Phys. Rev. B* **1991**, *44*, 498.
(31) Névot, L.; Croce, P. *Rev. Phys. Appl.* **1980**, *15*, 761.
(32) Wang, J.; Bedzyk, M. J.; Caffrey, M. *Science* **1992**, *258*, 775.
(33) Press, W. H.; Flannery, B. P.; Teukolsky, S. A.; Vetterling, W. T. *Numerical Recipes*, 1st ed.; Cambridge University Press: London, 1987.
(34) Parratt, L. G. *Phys. Rev.* **1954**, *95*, 359.

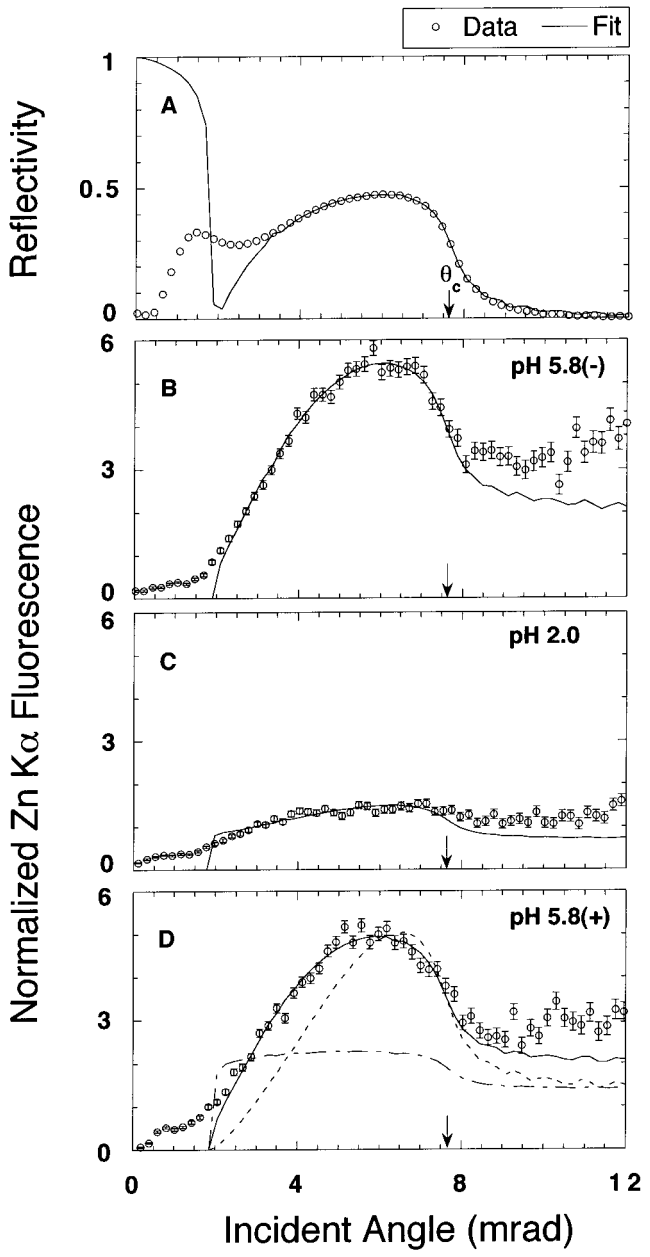

Figure 3. The experimental (circles) and theoretical (lines) angular dependence at 9.9 keV of the specular reflectivity at pH 5.8(−) (A) and the zinc Kα fluorescence yield at pH 5.8(−) (B), pH 2 (C), and pH 5.8(+) (D). The labels "−" and "+" indicate the direction in which the titration was performed. Thus, "−" indicates titration from high to low pH whereas "+" indicates the reverse. The reflectivity and angle were measured directly on an absolute scale. The fluorescence yields were normalized (i) to the same area of illuminated sample surface at all angles and (ii) to an incident beam intensity reading of 10^6 as monitored in the upstream ionization chamber (see text). This normalization means that the fluorescence intensities in B, C, and D are directly comparable. Also included in D are simulated fluorescence yield profiles based on different model zinc distribution profiles as follows: dot−dashed line, uniform zinc distribution ($L = \infty$); dashed line, condensed zinc layer at the membrane surface ($L = 0$, Helmholtz model) with no zinc in the bulk solution. These simulations are not normalized to the same amount of zinc in solution as in the case of pH 5.8(+).

values. The zinc Kα fluorescence profiles are all normalized to a fixed incident X-ray intensity (1 million counts in the upstream ionization chamber) so that the total amount of zinc ions in the solution at different stages in the pH titration can be compared directly.

Reflectivity and Solution Thickness. The reflectivity curve recorded at pH 5.8(−) along with the theoretical fit is presented in Figure 3A. The agreement between the experimental data and the fitting curves is remarkably good at $\theta > 3$ mrad. At lower incident angles ($\theta < 3$ mrad), the X-ray reflectivity profile shows several interesting features. For θ values up to 1.8 mrad, the critical angle for the overlayers (θ_{co}) at 9.9 keV, the prolene film and water layer can behave as a reflecting surface. Parenthetically, we note that the difference in the refractive index increment (δ) of the prolene film and electrolyte solution is so small that only a single critical angle, θ_{co}, was observed. Ideally, the reflectivity in this region is close to unity as the theoretical calculation predicts (solid line in Figure 3A). However, the upper surface of the prolene film is not perfectly flat and is best described by a mosaic model.[29] Hence, the incident angle of a collimated X-ray varies for the different domains making up the surface. Presumably, the angular variation can exceed θ_{co}. Therefore, part of the X-ray beam penetrates the air/film interface and is attenuated in the film and water layer. The observed reflectivity represents an integration of the reflectivity from all domains illuminated by the X-ray beam which, in the case of the mosaic model, can be significantly below that from a perfectly flat interface.

This angular variation is also responsible for the relatively shallow trough at ca. 2.0 mrad in the experimental reflectivity curve. If the air/film interface was perfectly flat, the reflectivity would approach zero because an antireflection or resonance condition is established when the incident angle is just above the critical angle of the film.[32] Additionally, as shown in eq 13, when θ approaches θ_{co}, d_o can be extremely large. In the same angular region, the attenuation of the X-ray beam in the overlayers is also maximized. If the upper surface of the prolene is not perfectly flat but of the mosaic type, the incident angle of the X-ray beam at each domain is different from the nominal incident angle where the resonance effect occurs. Again, the measured reflectivity represents an average over a range of incident angles, which has the effect of making the dip in the reflectivity profile at ca. 2.0 mrad less deep than expected for an ideally flat air/film interface.

In the reflectivity calculation shown in Figure 3A, the only imperfection included in the stratified model was the interfacial roughness as described above. The reflectivity curve calculation did not incorporate a mosaic surface model. This perhaps accounts for the less than perfect match between the theoretical calculation and the experimental reflectivity profiles below ca. 3 mrad. Fortunately, the unevenness of the prolene surface has a much reduced effect on the reflectivity data at higher angles. Beyond θ_{co}, both the prolene film and the solution layer can be considered more like an attenuation layer with little or no reflection. Additionally, the reflectivity and the fluorescence data in the higher angle region ($\theta >$ 3 mrad) contain most of the structural information that is of interest about the sample. Accordingly, the mismatch in the reflectivity curves below 3 mrad has a minimum impact on the reliability of the theoretical fits.

There are certain geometric factors that affect the shape of the reflectivity curve in the low-angle region. First, the sample intercepts an increasing portion of the 30 μm high beam as θ increases resulting in a linearly increasing reflectivity. At about 1.2 mrad, the length of the beam footprint equals the length of the sample (2.5 cm). Thereafter, the whole beam is intercepted by the sample. Second, a half-slit was positioned between the sample and the downstream ionization chamber to block the incident

Table 1. Parameters Best Describing Zinc Ion Distribution in the Diffuse Double Layer of a Zinc Chloride Solution in Contact with a Phospholipid Membrane as a Function of pH[a]

pH	d_w (μm)	z_0 (Å)	L (Å)	N_s (mM)	r (%)
5.8(−)	1.37 (±0.02)	19 (+3, −3)	20 (+3, −4)	122 (+80, −30)	68
4.2(−)	1.21 (±0.02)	22 (+4, −5)	18 (+4, −5)	37 (+25, −10)	41
2.0(−)	0.90 (±0.02)	18 (+7, −15)	9 (+9, −8)	19 (+19, −7)	21
4.2(+)	1.22 (±0.02)	15 (+4, −5)	19 (+4, −5)	33 (+25, −10)	39
5.8(+)	1.23 (±0.02)	19 (+3, −3)	19 (+3, −4)	115 (+80, −30)	70

[a] Parameters obtained using the XSW analysis as described in the text are as follows: d_w, the electrolyte solution thickness; z_0, charged surface to mirror distance; L, ion Debye length; N_s, the zinc surface concentration; r, the percentage of total zinc in the diffuse double layer. The concentration of zinc chloride in the bulk solution (N_b) is 0.1 mM.

beam. The top of the blade was located ca. 200 μm above the top of the direct incident X-ray beam. Thus, at low angles, part of the reflected beam was masked by the slit and the measured reflectivity is artificially low. As θ increased, an increasing fraction of the reflected beam passed over the slit blade into the ion chamber and was counted. These low-angle geometric factors have no effect on the fluorescence measurement and have not been corrected for in the reflectivity calculation.

The linear absorption coefficients of the prolene film and the solution layer are 1.8 and 5.3 cm^{-1} at 9.9 keV, respectively. With a prolene film thickness of 4.2 μm specified by the manufacturer, the χ^2-fit of the reflectivity curve indicated that the solution thickness (d_w) was 1.37 ± 0.02 μm. The sensitivity of the fit to the solution thickness will be addressed under Discussion.

Fluorescence Yield Profiles and Zinc Distribution. The zinc Kα fluorescence profile at pH 5.8(−) is shown in Figure 3B. A single peak in the angle range from 3 to 6 mrad suggests that there was a concentrated zinc layer close to the membrane surface and that the center of mass of this layer was less than $D_c/2$, that is, ca. 40 Å from the mirror surface. The fluorescence yield peak is relatively broad because the concentrated zinc layer has an associated finite distribution and because of the contribution of zinc in the 1.37 μm thick bulk electrolyte solution. A χ^2-fit shows that the concentrated layer with an exponentially decaying distribution (see eq 15) amounted to 68% of the total zinc in the electrolyte solution. Zinc, uniformly distributed in the 1.37 μm thick bulk solution, made up the remaining 32%. This suggests that a substantial fraction of the phospholipid headgroups were deprotonated at the relatively high pH of 5.8. The optimum χ^2-fit to the experimental fluorescence data shows the following parameters: the distance between the surface-condensed layer and the gold mirror surface (z_0) is 19 Å, the ratio between the surface zinc concentration and the bulk concentration (N_s/N_b) is 1.22×10^3, and the ion distribution decay length (or the effective Debye length, L) is 20 Å. Assuming that the zinc concentration in the bulk solution is 0.1 mM, the surface zinc concentration should be 122 mM.

After the pH value in the bathing electrolyte solution was lowered to 4.2, the height of the fluorescence peak (data not shown) decreased corresponding to a smaller amount of zinc in the diffuse double layer. At this pH, the concentrated zinc layer represented ca. 41% of total amount of zinc in the solution. The fitting parameters show that the concentrated zinc layer had a similar distribution ($z_0 = 21$ Å and $L = 18$ Å) as that at pH 5.8(−) but with a much lower surface concentration ($N_s = 37$ mM).

When the solution pH was decreased further to pH 2.0(−), the fluorescence signal (Figure 3C) became extremely weak and almost flat in the region between 3.0 and 7.5 mrad. In this case, the majority of the zinc was found distributed uniformly in the bulk solution. Only 21% of the zinc was in the concentrated layer at this low pH value. The fitting results show that under these conditions $N_s = 19$ mM, $z_0 = 18$ Å, and $L = 9$ Å. These results agree qualitatively with those obtained previously using a similar membrane/aqueous interface system.[17] However, at such low surface ion concentration, the χ^2-fit is sensitive only to the amount of zinc ion but quite insensitive to the fitting parameters N_s, z_0, and L which are found to be strongly correlated. Therefore, the value of the latter parameters describing the diffuse double layer in solution at this low pH is uncertain.

Reversible Formation of the Diffuse Double Layer. The results presented above show that upon acid titration, the actual distribution of the diffuse double layer changes in a dramatic and predictable manner. If the process is thermodynamically reversible, it should be possible to recover the original diffuse double layer profile upon back-titration. This is supported by the data in Figure 3D which shows the zinc fluorescence yield profile for the same sample as used to collect the data shown in Figure 3A−C after the zinc chloride bathing solution was titrated back from a pH value of 2.0 to a value of 5.8. The peak fluorescence intensity is fully recovered, and the fluorescence yield profile is almost identical to that observed at the original pH value of 5.8 at the beginning of the experiment (Figure 3B). The fit to the experimental data shows a surface zinc concentration of 115 mN and an effective Debye length of 19 Å. During back-titration to pH 5.8, the XSW measurement was also performed at pH 4.2(+). The fluorescence recovery at this pH value (data not shown) was ca. 75% of that observed at pH 4.2(−). This incomplete recovery suggests that the change of the diffuse double layer responding to the pH change in the solution can be time-dependent (hysteresis). After the XSW measurement at pH 2.0(−) was finished, the sample was soaked with the pH 4.2(+) solution for about 20 min. For the scans at pH 5.8(+), the incubation time was in excess of 6 h because of an unexpected synchrotron beam-dump.

The measured parameters obtained from the XSW analysis, including d_w, z_0, L, N_s, and the ratio between the amount of zinc in the diffuse double layer and total zinc encapsulated in the zinc chloride bathing solution, are listed in Table 1 as a function of pH during the course of acid and base titration. The spatial distribution of zinc in the solution next to the phospholipid membrane shown in Figure 4 is based on these measured parameters. All distances are referenced to the charged membrane surface, that is, the membrane/aqueous interface. The data in Table 1 and Figure 4 attest to the reversibility of the zinc distribution upon changing the pH of the electrolyte solution.

The fitting results show that at all pH values, z_0 is considerably smaller (by ca. 20 Å) than expected from ellipsometry measurements. The disparity could arise from differences in the methodologies used and their respective limitations, from possible penetration of the electrolyte solution into the lipid monolayer, from possible

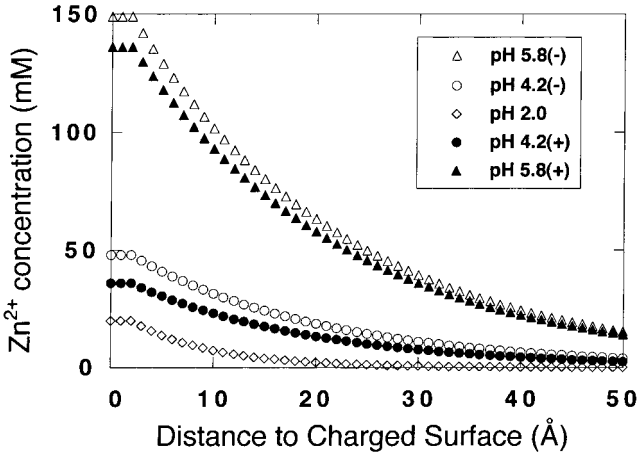

Figure 4. Spatial distribution of zinc ions in the electrolyte solution at and next to the charged membrane surface at the indicated pH values. The distribution profiles correspond to plots of eq 15 incorporating the best fitting parameters from XSW measurements as presented in Table 1. The distribution data were calculated at an interval of 1 Å. All the distribution curves originate at the membrane surface ($z_0 = 0$). The concentration of zinc chloride in the bulk solution is 0.1 mM.

damage of the lipid monolayer during acid washing, and/or from electrolyte solution induced tilting of the lipid adlayer. However, because the ion distribution in the diffuse double layer was found to be reversible, a stable charged phospholipid layer surface must always have been present throughout the experiment.

Error Assessment. The χ^2-fit of the fluorescence data involves multiple fitting parameters. Under certain circumstances, for example, at low pH values, these parameters are strongly correlated. Therefore, it is especially important to discuss the confidence level for all the fitting parameters. In what follows, we present the method used to estimate the errors for the χ^2-fit.

The number of parameters (K) used to fit the fluorescence data is 3. These parameters were used to fit a total of 29 experimental data points (M). The number of degrees of freedom N, defined as $M - K$, is 26. It was found that the minimum χ^2 at all pH values was always close to N, implying a moderately good fit.[33]

To estimate the error associated with each parameter, the following systematic method was used. At the minimum χ^2, identified as χ_0^2, the set of three optimal fitting parameters, symbolized by a_i ($i = 1, 2, 3$), is the starting point. For example, to find the (+) and (−) errors associated with a_1, the value of a_1 is changed incrementally by $\pm\Delta a_1$ from its optimal value. Then, new values, a_2 and a_3, are found where χ^2 is minimized at χ_1^2. With a sufficiently large Δa_1^{max}, $\Delta\chi^2$ ($= \chi_1^2 - \chi_0^2$) reaches 6.3 representing the 90% confidence level for a 3-parameter fitting[33]. The value of Δa_1^{max} is taken as the error for a_1. This procedure is repeated for every fitting parameter.

It was found that for all the parameters, $\Delta\chi^2$ increases monotonically with increasing Δa_i. This indicates that the parameter set obtained from the χ^2-fit is the true optimal set for the given fitting model. However, we also note that the plus/minus error bars for each parameter are not identical perhaps reflecting a correlation that exists between the fitting parameters. It is clearly shown in Table 1 that the relative errors at higher pH values (5.8 and 4.2) are much smaller than those at pH 2.0. This suggests that the correlation between the fitting parameters N_s, z_0, and L is much reduced at higher pH.

Table 2. Equivalent Surface Density of the Total Amount of Zinc Ion in the Diffuse Double Layer and Estimated Surface Bound Zinc Concentration at Different Bulk Solution pH Values

	zinc surface density (10^{12} ions/cm^2)	
pH	equivalent in diffuse double layer[a]	surface bound[b]
5.8(−)	14.7	2.2
4.2(−)	4.01	0.67
2.0(−)	1.71	0.34
4.2(+)	3.78	0.59
5.8(+)	13.2	2.1

[a] These values were determined from the data in Table 1 as N_s(mM) × 6.022 × 10^{17} ions cm^{-3} mM^{-1} × L(Å) × 10^{-8} cm Å^{-1}. [b] Surface density of bound zinc in units of ions/cm^2 was estimated as N_s(mM) × 6.022 × 10^{17} ions cm^{-3} mM^{-1} × 3(Å) × 10^{-8} cm Å^{-1} where the bound zinc is a confined layer of 3 Å thick.

Discussion

Surface Charge Density and Reversibility. The equilibrium condition at the negatively charged lipid membrane is dictated by the binding competition between the positively charged hydrogen and zinc ions. The zinc surface density can be determined approximately from the zinc distribution obtained from the XSW measurement. Shown in Table 2 is the equivalent surface density of the total amount of zinc in the diffuse double layer. Also presented in Table 2 is the estimated surface bound zinc concentration. This estimation is based on the assumption that the condensed zinc layer on the membrane surface, if there is such a layer, has a thickness of ca. 3 Å corresponding to the ionic diameter of zinc (zinc ions have a diameter ranging from 1.2 to 1.5 Å in crystals[35]). These data show that the bound zinc at the membrane surface accounts for only a small fraction of the total that exists in the concentrated layer. Furthermore, a surface concentration of $N_s = 122$ mM corresponds to a zinc surface density of 2.20 × 10^{12} ions cm^{-2} at pH 5.8(−). Assuming that the phospholipid has a molecular area of ca. 40 Å^2 (2.5 × 10^{14} molecules cm^{-2}, from the surface area−pressure isotherm of the phospholipid monolayer at the air/water interface, data not shown) at the membrane/aqueous interface, the condensed zinc layer at the membrane surface is equivalent to only 0.88% of a phospholipid monolayer. In other words, the concentrated zinc layer has, on average, ca. 1 zinc ion associating with each 100 phospholipid headgroups at pH 5.8(−). The zinc ion/headgroup ratio drops to ca. 1/700 at pH 2.0(−). Therefore, the process observed in this study upon changing pH is associated with the protonation/deprotonation of the membrane headgroup, which gives rise to a reversible zinc distribution in the electrolyte solution. The zinc ion concentration in the diffuse double layer is extremely sensitive to the charge density at the membrane surface and is solely dependent on the electrostatic potential in the aqueous solution. It is demonstrated clearly in this study that ion distribution in the diffuse double layer and, by implication, the degree of lipid headgroup protonation are fully reversible thermodynamically.

As noted above, the total charge associated with zinc ions in the diffuse double layer should equal the net surface charge on the membrane at pH 5.8 assuming that the contribution of H^+ in the diffuse double layer is negligible at this relatively high pH (pH 5.8 ≡ 1.59 μM H^+). If H^+ is bound to the remaining headgroup to effect overall charge neutrality, the protonation level of the membrane

(35) Shannon, R. D. *Acta Crystallogr.* **1974**, *A32*, 751.

surface can be calculated based on an estimated lipid surface density of 2.5×10^{14} cm^{-2}. At pH 5.8(−), a zinc density of 1.47×10^{13} cm^{-2} in the diffuse double layer, as shown in Table 2, implies that approximately 88% of the phospholipid headgroups are in the protonated state. Therefore, the effective pK_a of this phospholipid headgroup in monolayer form is greater than 5.8. To our knowledge, the pK_a of the latter has not been reported. However, a homologue, dihexadecyl hydrogen phosphate (dicetyl phosphate), has been found to have a pK_a value of 4.5 when measured in multilamellar vesicles dispersed with phosphatidylcholine and cholesterol.[36] The presence of the latter neutral lipids, which act as surface spacers, serves to depress the pK_a. Thus, the value in a pure phospholipid monolayer is expected to be higher in line with the estimated pK_a value of >5.8 reported above.

Debye Length. As illustrated in Table 1, the zinc ion Debye length, L, varies from 10 to 20 Å in the pH range from 2 to 6. The diffuse double layer theory predicts an L value which is an order of magnitude larger under these same conditions (L = 176 Å at 0.1 mM $ZnCl_2$ and 25 °C). To what can we ascribe the disparity? The first and most obvious point of difference concerns the likely inadequacy of a one-dimensional PB equation as a means for describing a discretely charged surface as obtains in the present study (see Background). The second has to do with the possible perturbing effect that an adjacent conducting gold mirror surface has on the diffuse double layer itself. The reader's attention is drawn to the fact that the measured Debye length is comparable to the distance between the mirror and the charged surface (Table 1). These questions, although not resolved in the current study, suggest additional experiments to advance our understanding of the diffuse double layer. Thus, the XSW method can be used to monitor with exquisite sensitivity the effects on the diffuse double layer profile of surface charge density, ionic strength, and the mirror to charged surface distance. The latter would make effective use of ionic polymer brushes of varying chain lengths.

Sensitivity of the XSW Analysis. Under Results, we have shown that the agreement between the experimental data and the theory is good in the angle range between 3.0 and 8.0 mrad for both the reflectivity and fluorescence yield profiles. The goodness of this fit allows us to reliably characterize the structure of the diffuse double layer in solution. To our knowledge, this work represents the first of its kind in which the variable period XSW generated above a gold mirror was used as a structure probe to investigate the reversibility of the diffuse double layer at a membrane/aqueous interface. By way of evaluating the reliability of the method, it is necessary to show the sensitivity of the XSW analysis to the structure of the system under investigation. Specifically, we must address the sensitivity of the analysis to the thickness of the electrolyte solution layer and to the zinc distribution in the vicinity of the membrane surface.

For this purpose, both the reflectivity and fluorescence data at pH 5.8(−) along with the corresponding best fit in the angle range of 3.0−8.0 mrad are presented in Figure 5. Also included in the figure are several theoretical profiles calculated using different values of the fitting parameters. In Figure 5A, for example, the reflectivity calculation was made with a solution thickness 500 Å larger (dotted line) than that yielding the best fit (solid line) while the other parameters remained unchanged. This resulted in a dramatically increased χ^2 value, and the overall mismatch between the fit and the experimental data is quite obvious upon inspection. We emphasize here that the calculation demonstrates the sensitivity of the reflectivity to the electrolyte solution thickness assuming that the calculated refractive index and the thickness of the prolene layer and the refractive index of the gold mirror are exactly known. Therefore, the accuracy of the water layer thickness is limited by the accuracy of these parameters. Uncertainty in the values of these parameters may introduce an error in the solution layer thickness but by a fixed amount (less than 2000 Å) because the same prolene film and mirror were used throughout the measurement

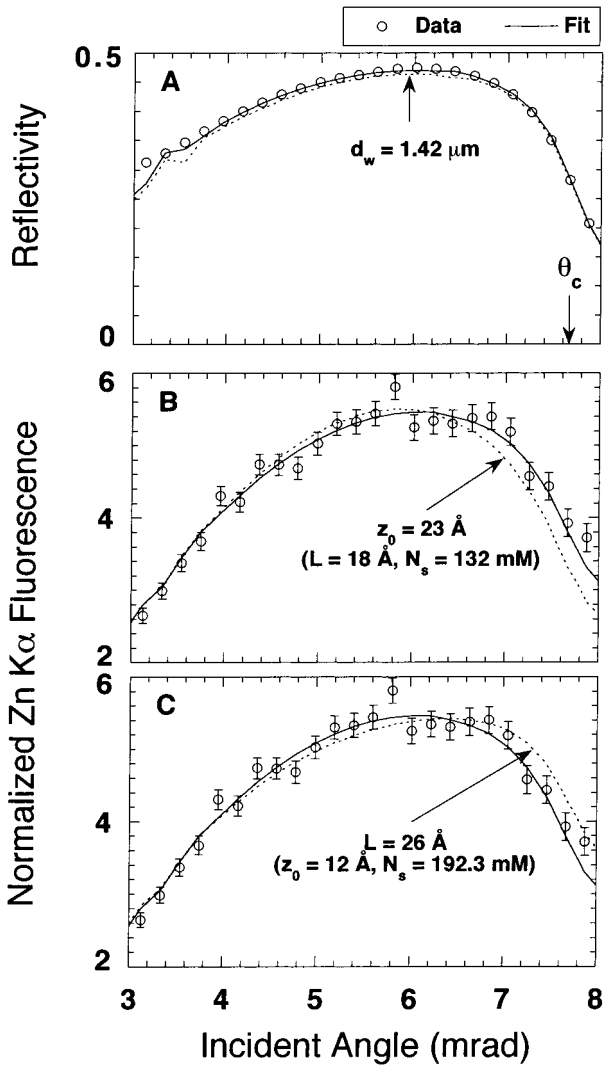

Figure 5. Sensitivity of the reflectivity (A) and fluorescence profiles (B and C) to the structure of the diffuse double layer at pH 5.8(−). The experimental data (circles) and the best fit (solid line) were taken from the 3−8 mrad region of Figure 3A,B. For the reflectivity profile, the best fitting solution thickness (d_w) is 1.37 μm. A calculated reflectivity curve using d_w = 1.42 μm is included for comparison (dashed line in A). While all other parameters such as prolene film thickness and refractive index remain fixed, the effect of the additional 500 Å in solution thickness is to reduce reflectivity to a small but significant degree. In the case of the zinc Kα fluorescence yield profile, the best fit (solid lines in B and C) was obtained with z_0 = 19 Å and L = 20 Å. Theoretical curves generated using z_0 = 23 Å (dashed line in B) and L = 26 Å (dashed line in C) are included for comparison. To generate these theoretical curves, all fitting parameters except z_0 or L for B or C, respectively, were allowed to change by way of minimizing χ^2. The corresponding "best fitting" parameter values are shown in the parentheses.

(36) Maitani, Y.; Nakagaki, M.; Nagai, T. *Int. J. Pharm.* **1990**, *64*, 89.

series. Finally, there is one other experimental limitation that may affect the accuracy in determining the solution layer thickness as follows. Because the electrolyte solution trapped between the gold mirror and the prolene film was under a continuous, slightly negative pressure (see Methods), the thickness of this solution layer may decrease during the course of the experiment. By comparison of the reflectivity curves of several sequential scans at a given pH value (normally over a period of 3−6 h), the thickness reduction of the solution ranged from 0 to 1000 Å. The corresponding mean value was used in subsequent data analysis.

In the case of the fluorescence data at pH 5.8(−), the best fit is achieved with $z_0 = 19$ Å and $L = 20$ Å. If either z_0 or L is increased by 5 or 6 Å, respectively, as is shown in Figures 5B,C, the quality of the fit deteriorates noticeably. Parts B and C of Figure 5 show the optimal fitting result when z_0 is fixed at 24 Å or L is fixed at 26 Å, respectively, while the other fitting parameters are allowed to change. The χ^2-minimum in the two simulations is 41.6 and 39.5, respectively, whereas the best fit shown in Figure 3B has a χ^2 value of 23.2. Under the condition of high pH when a high ion concentration is established close to the electrolyte/membrane interface, the data in Figure 5 show that the XSW analysis offers good spatial resolution, on the order of angstroms, in defining the diffuse double layer profile which can extend from the charged membrane surface for several micrometers. With a lower diffuse double layer concentration, the X-ray standing wave spatial resolving power is considerably lessened.

We note that beyond the critical angle of the gold mirror ($\theta_c = 7.67$ mrad), the mismatch between the fit and the experimental fluorescence yield data is obvious (see Figure 3B−D). Specifically, the experimental data are consistently higher than the fitting curve. This mismatch is ascribed partly to the poorer counting statistics as a result of a low counting rate and a high scattering background at high angles. On the other hand, because the fluorescence intensity above θ_c is a quantitative measure of the total amount of zinc in the sample within the footprint of the X-ray beam, the discrepancy between the fit and experimental curve implies the presence of extra zinc besides that in the electrolyte solution, that is also being interrogated by the X-ray beam. By subtracting the fit value from the experimental data at each data point (data not shown), we found that the mismatch is a minimum below θ_c and increases abruptly as soon as the incident angle reaches θ_c. The mismatch increases monotonically thereafter. Because the X-rays penetrate the mirror surface at $\geq\theta_c$, these data suggest that there is a trace of zinc impurity in the mirror substrate which consists of gold and chromium layers on a piece of float glass (see Figure 1). Above θ_c, the incident X-rays penetrate the mirror surface and excite the zinc impurities residing inside the substrate. A comparison between the magnitude of the mismatch and zinc fluorescence intensity from the diffuse double layer reveals that the level of zinc contamination in the sampled substrate is on the order of ca. 1% of a monolayer assuming a zinc area density of 2.5×10^{14} atoms cm^{-2}.

Reliability of the XSW Analysis. Although the XSW measurement is extremely sensitive to the diffuse double layer distribution at relatively high pH values, we acknowledge that the theoretical fitting procedure is, to a certain extent, model-dependent. For example, one side of a Gaussian as opposed to an exponentially decaying function can be used to model the spatial distribution of the concentrated zinc layer near the membrane surface without sacrificing the goodness of fit as judged by the calculated χ^2 values. The fitting parameters in the Gaussian model distribution are the peak position z_0', the peak half-width at half-height (HWHH) about the peak position L' and the peak height N_s^2 normalized by the bulk zinc concentration N_0. The best fit to the data at pH 5.8(−) with the Gaussian distribution model gives the following parameters: $z_0' = 22$ Å, $L' = 21$ Å, and $N_s = 135$ mM. For such a distribution, zinc in the concentrated layer accounts for ca. 78% of the total zinc in the bathing solution. If one considers that the Gaussian half-width is analogous to the decay length in the exponential function (eq 15) as a parameter that describes the distribution width of the concentrated zinc layer, the Gaussian and the exponential models give very similar results. Further, the position parameter z_0' (22 Å) in the Gaussian model and the position of the surface bound zinc layer z_0 (19 Å) at pH 5.8(−) in the exponential model in eq 15 characterize the position at which the most concentrated zinc layer was found above the mirror surface. The difference between z_0' and z_0 is only 3 Å which is close to the sensitivity limit of the XSW analysis in the current application. Therefore, the zinc distributions presented in this study are reliable and realistically reflect ion distribution in the diffuse double layer within the spatial resolution limits of a few angstroms afforded by this method.

Radiation Damage. Because of the need for relatively long exposure times to accumulate satisfactory counting statistics, the possibility of the sample succumbing to radiation damage must be addressed. We conclude that radiation damage is not a problem based on the following observation. Ion distribution in the diffuse double layer adjacent to the membrane surface was almost completely recovered at the end of the experiment upon back-titration to pH 5.8(+). Because the sample was not moved with respect to the X-ray beam during the course of the study, the radiation effects on the phospholipid membrane are not important under current experimental conditions. In addition to being resistant to ionizing radiation, the polymerized phospholipid monolayer appears to be insensitive to the extensive and repeated washings with a variety of solutions including the relatively acid pH 2.0 solution. Parenthetically, we note that X-radiation damage can be limiting not only in the case of thin films of the type used in this study but also with hydrated bulk lipid samples.[37−40]

Selection of the Mirror Materials. The XSW method is currently limited to measuring the distribution of ions having X-ray fluorescence energies high enough to penetrate through the bathing electrolyte solution layer and the encapsulating plastic film. Accordingly, the choice of X-ray mirror material is crucial to the success of these measurements. Both the plastic and aqueous solution layers behave as X-ray reflecting mirrors below 1.8 mrad such that the liquid layer is not exposed in a significant way to the X-ray beam in the angle range from 0 to 1.8 mrad. With reference to the reflectivity curve in Figure 3A, the trough at around 2 mrad marks the angle at which the incident X-rays penetrate fully through the liquid and prolene layers. Therefore, the usable fluorescence data can be collected in the angle range from ca. 2.5 mrad to the critical angle of the solid substrate. A wider usable angular range, which implies more angular steps, more data points, and better resolution in the experiment,

(37) Caffrey, M. *Nucl. Instrum. Methods* **1984**, *222*, 329.
(38) Cheng, A.-C.; Hogan, J. L.; Caffrey, M. *J. Mol. Biol.* **1993**, *229*, 291.
(39) Cheng, A.; Caffrey, M. *Biophys. J.* **1996**, *70*, 2212.
(40) Cherezov, V.; Cheng, A.; Petit, J.-M.; Diat, O.; Caffrey, M. *Cell. Mol. Biol.* **2000**, *46*, 1133.

provides better accuracy and reliability for the XSW measurement. To maximize this angular range, it is desirable to have the electron density contrast between the substrate and aqueous overlayer and the plastic film as large as possible. A gold mirror fits the bill by providing a relatively wide angular window of ca. 5 mrad (2.5−7.5 mrad) in which to collect useful data. This is in contrast to the rather limited window of only ca. 2 mrad available in our previous study when a Si/W LSM was used as the X-ray mirror and solid substrate for the organic monolayers.[17]

Conclusions

A variable period XSW generated by external reflection from a gold mirror has been used in an element-specific manner to measure zinc ion distribution in an electrolyte solution in contact with a negatively charged lipid membrane surface during the course of a pH titration cycle in the bathing solution. The zinc distribution in the diffuse double layer was determined in situ by means of an XSW-induced X-ray fluorescence measurement. The results show that the ion distribution at the charged membrane/electrolyte interface is reversible upon proton titration in the electrolyte solution in the pH range between 2 and 5.8. In qualitative agreement with the Gouy−Chapman theory, the interaction between the membrane surface and the zinc ions in the diffuse double layer is dominated by electrostatic interactions. This experiment demonstrates the effectiveness of the XSW method as a means for measuring, in a most direct way, ion distribution in such a complex system. With this method in hand and its utility clearly established, we have ahead of us almost a century's worth of theory to set about testing experimentally. Indeed, the approach is applicable to a wide variety of charged and uncharged solutes and surfaces where the X-ray fluorescence properties of the probe atom or ion match the optical characteristics of the X-ray mirror surface and the dispersing medium.

Acknowledgment. The help and support of the entire CHESS (National Science Foundation Grant DMR 12822) staff is acknowledged. Many thanks go to G. M. Bommarito for invaluable advice regarding both theoretical and experimental aspects of this work. We also thank S. Kirchner for his comments on the manuscript. This work was supported by grants from the National Institutes of Health (DK 36849, DK 46295, GM56969, and GM61070), the National Science Foundation (DIR-9016683), and the Petroleum Research Fund of the American Chemical Society (30537-AC7) to M.C. and by a Presidential Fellowship from The Ohio State University to J.W. who is also partly supported by the U.S. Department of Energy, under Contract W-31-109-Eng-38.

LA001542X